arXiv:1604.01986v1 [astro-ph.GA] 7 Apr 2016

Upper Limit on Star Formation and Metal Enrichment in Minihalos

Renyue Cen[1]

ABSTRACT

An analysis of negative radiative feedback from resident stars in minihalos is performed. It is found that the most effective mechanism to suppress star formation is provided by infrared photons from resident stars via photo-detachment of H^-. It is shown that a stringent upper bound on (total stellar mass, metallicity) of ($\sim 1000\,\mathrm{M}_\odot$, -3.3 ± 0.2) in any newly minted atomic cooling halo can be placed, with the actual values possibly significantly lower. This has both important physical ramifications on formation of stars and supermassive black seeds in atomic cooling halos at high redshift, pertaining to processes of low temperature metal cooling, dust formation and fragmentation, and direct consequences on the faint end galaxy luminosity function at high redshift and cosmological reionization. The luminosity function of galaxies at the epoch of reionization may be substantially affected due to the combined effect of a diminished role of minihalos and an enhanced contribution from Pop III stars in atomic cooling halos. Upcoming results on reionization optical depth from Planck High-Frequency Instrument data may provide a significant constraint on and a unique probe of this star formation physical process in minihalos. As a numerical example, in the absence of significant contributions from minihalos with virial masses below $1.5\times10^8\,\mathrm{M}_\odot$ the reionization optical depth is expected to be no greater than 0.065, whereas allowing for minihalos of masses as low as ($10^7\,\mathrm{M}_\odot$, $10^{6.5}\,\mathrm{M}_\odot$) to form stars unconstrained by this self-regulation physical process, the reionization optical depth is expected to exceed $(0.075, 0.085)$, respectively.

1. Introduction

Star formation in minihalos is a fundamental issue, because it is responsible for enriching the primordial gas with first metals that shape the subsequent formation of stars and possibly supermassive black hole seeds in atomic cooling halos. Since the pioneering works (e.g., Abel et al. 2002; Bromm et al. 2002; Nakamura & Umemura 2002), most studies have focused on formation of individual stars (e.g., Hirano et al. 2014). So far studies of the effects of external Lyman-Werner band (LW) ($h\nu = 11.2 - 13.6$eV) radiation background (e.g., Machacek et al. 2001; Wise & Abel 2007; O'Shea & Norman 2008), external IR radiation background (e.g., Chuzhoy et al. 2007; Hirano et al. 2015) on gas chemistry and thermodynamics hence star formation in minihalos have produced significant physical insight. We assess the effects of these two - LW photo-dissociation and IR photo-detachment - H_2 formation suppressing processes due to resident stellar population within minihalos, instead of the respective collective

backgrounds widely considered. We show that photo-detachment process of H_2 by infrared photons of energy $h\nu \geq 0.755$eV produced by resident stars places a strong upper bound on stellar mass and metals that may be formed in minihalos. This upper limit needs to be taken into account in the general considerations of galaxy formation at high redshift.

2. Maximum Stellar Mass and Metal Enrichment in Minihalos

Minihalos are defined as small dark matter halos with virial temperature below that for efficient atomic cooling (i.e., $\mathrm{T_v} \leq 10^4$K). Minihalos form early in the standard cold dark matter model and are only relevant for high redshift. Star formation may start in minihalos with $\mathrm{T_v}$ as low as ~ 1000K or so. The relation between halo virial mass ($\mathrm{M_v}$) and virial temperature ($\mathrm{T_v}$) is

$$M_{\rm v} = 10^8 h^{-1}\,{\rm M}_\odot \left(\frac{T_{\rm v}}{1.98\times 10^4 K}\right)^{\frac{3}{2}} \left(\frac{0.6}{\mu_P}\right)^{\frac{3}{2}} \left(\frac{\Omega_{\rm m}}{\Omega_m^z}\frac{\Delta_c}{18\pi^2}\right)^{-\frac{1}{2}} \left(\frac{1+z}{10}\right)^{-\frac{3}{2}}, \quad (1)$$

where z is redshift, Ω_m and Ω_Λ are density parameter and cosmological constant at redshift zero, respectively; $\Omega_m^z \equiv [1+(\Omega_\Lambda/\Omega_m)(1+z)^{-3}]^{-1}$ is the density parameter at redshift z; $\Delta_c = 18\pi^2 + 82d - 39d^2$ and $d = \Omega_m^z - 1$ (see Barkana & Loeb 2001 for more details). The corresponding physical virial radius is

$$r_{\rm v} = 0.784{\rm h}^{-1}{\rm kpc} \left(\frac{T_{\rm v}}{1.98\times 10^4 K}\right)^{\frac{1}{2}} \left(\frac{0.6}{\mu_P}\right)^{\frac{1}{2}} \left(\frac{\Omega_{\rm m}}{\Omega_m^z}\frac{\Delta_c}{18\pi^2}\right)^{-\frac{1}{2}} \left(\frac{1+z}{10}\right)^{-\frac{1}{2}}. \quad (2)$$

In minihalos at high redshift, molecular hydrogen H_2 is the primary gas cooling agent, before a significant amount of metals is present. In the absence of a significant amount of dust grains, the dominant H_2 formation channel is via a two-step gas phase process (e.g., Draine 2003), first with radiative association:

$$\mathrm{H} + e^- \rightarrow \mathrm{H}^- + h\nu, \quad (3)$$

followed by associative detachment:

$$\mathrm{H}^- + \mathrm{H} \rightarrow \mathrm{H}_2 + e^-. \quad (4)$$

Given this formation channel, if one is interested in suppressing H_2 formation, there are two main ways to achieve that goal. One is by destruction of formed H_2 molecules through the photo-dissociation process by photons in the LW band of $h\nu = 11.2 - 13.6$eV:

$$\mathrm{H}^2 + h\nu \rightarrow \mathrm{H} + \mathrm{H}. \quad (5)$$

The other is by reducing the density of H^-, to which the rate of H_2 formation is proportional, by infrared (IR) photons of energy $h\nu \geq 0.755$eV via the photo-detachment process:

$$\mathrm{H}^- + h\nu \rightarrow \mathrm{H} + e^-. \quad (6)$$

For simplicity, we assume that the initial mass function (IMF) of Population III (Pop III) stars has a powerlaw distribution of the same Salpeter slope:

$$\mathrm{n}(\mathrm{M}_*)\mathrm{dM}_* = \mathrm{CM}^{-2.35}\mathrm{dM}_*, \tag{7}$$

with an upper mass cutoff $100\,\mathrm{M}_\odot$ and a lower mass cutoff $\mathrm{M}_{\rm low}$ that we will vary to understand its influence on the results; C is a constant normalizing the stellar abundance per unit of star formation rate. We stress that our results are rather insensitive to either $\mathrm{M}_{\rm low}$ or the slope of the IMF. Then, one can compute the intrinsic spectral luminosity (in units of $\mathrm{erg\ sec^{-1}\ Hz^{-1}\ sr^{-1}}$) per stellar mass at any photon energy ν as

$$\mathrm{L}_\nu = \int_0^{\mathrm{t_h}} \int_{\mathrm{L_{low}}}^{100\,\mathrm{M}_\odot} \theta(\mathrm{t_{ms}} - \mathrm{t_h} + \mathrm{t_f})\dot{\mathrm{M}}_*(\mathrm{t_f})\mathrm{J}_\nu(\mathrm{M}_*)\mathrm{n}(\mathrm{M}_*)\mathrm{dM}_*\mathrm{dt_f}, \tag{8}$$

where $\mathrm{J}_\nu(\mathrm{M}_*)$ is the mean spectral luminosity of a star of mass M_* at photon energy $h\nu$ in the main sequence; $\theta(x)$ is the Heaviside theta function; $\mathrm{t_{ms}}(\mathrm{M}_*)$ is the star's main sequence lifetime; $\mathrm{t_f}$ and $\mathrm{t_h}$ are the formation time of the star in question and the time under consideration when the luminosity is computed; $\dot{\mathrm{M}}_*(\mathrm{t_f})$ is star formation rate at time $\mathrm{t_f}$.

The left panel of Figure 1 shows the individual intrinsic Pop-III stellar black-body spectrum per unit stellar mass times the main sequence lifetime for a range of masses for individual Pop III stars (indicated in the legend in units of solar mass), based on data from Marigo et al. (2001). It is easy to see that low mass stars are more efficient producers of IR photons (indicated by the vertical dashed magenta line); for $1\,\mathrm{M}_\odot$ to $20\,\mathrm{M}_\odot$, a decrease of approximately 100 for IR intensity per unit stellar mass is observed. For the LW band photons (indicated by the two vertical dashed black lines), the opposite holds: a decrease of approximately four orders of magnitude is seen from $20\,\mathrm{M}_\odot$ to $1\,\mathrm{M}_\odot$. In the right panel of Figure 1 we show comparisons the IR (LW) intensities of a single star of mass indicated by the x-axis in magenta (black) solid curves for redshifts $z = 25$ ($z = 7$), to be compared to the the threshold intensities for completion suppression of H_2 formation by the respective processes shown as the horizontal dashed lines with the corresponding colors. See below for how the the threshold intensities are computed.

Wolcott-Green & Haiman (2012) show that complete suppression of H_2 formation in mini-halos at high redshift is possible by either LW photo-dissociation or IR photo-detachment process. Based on a detailed modeling, they derive a critical radiation intensity for complete suppression of H_2 formation of

$$\mathrm{J_{LW,crit}} = 1.5 \times 10^{-21}\mathrm{ergs^{-1}cm^{-2}Hz^{-1}sr^{-1}} \tag{9}$$

at the LW band via photo-dissociation process alone, and a critical radiation intensity of

$$\mathrm{J_{IR,crit}} = 6.1 \times 10^{-20}\mathrm{ergs^{-1}cm^{-2}Hz^{-1}sr^{-1}} \tag{10}$$

at the IR band ($h\nu = 2$eV) via photodetachment process alone, under the assumption of the existence of the respective backgrounds, *not* internal radiation.

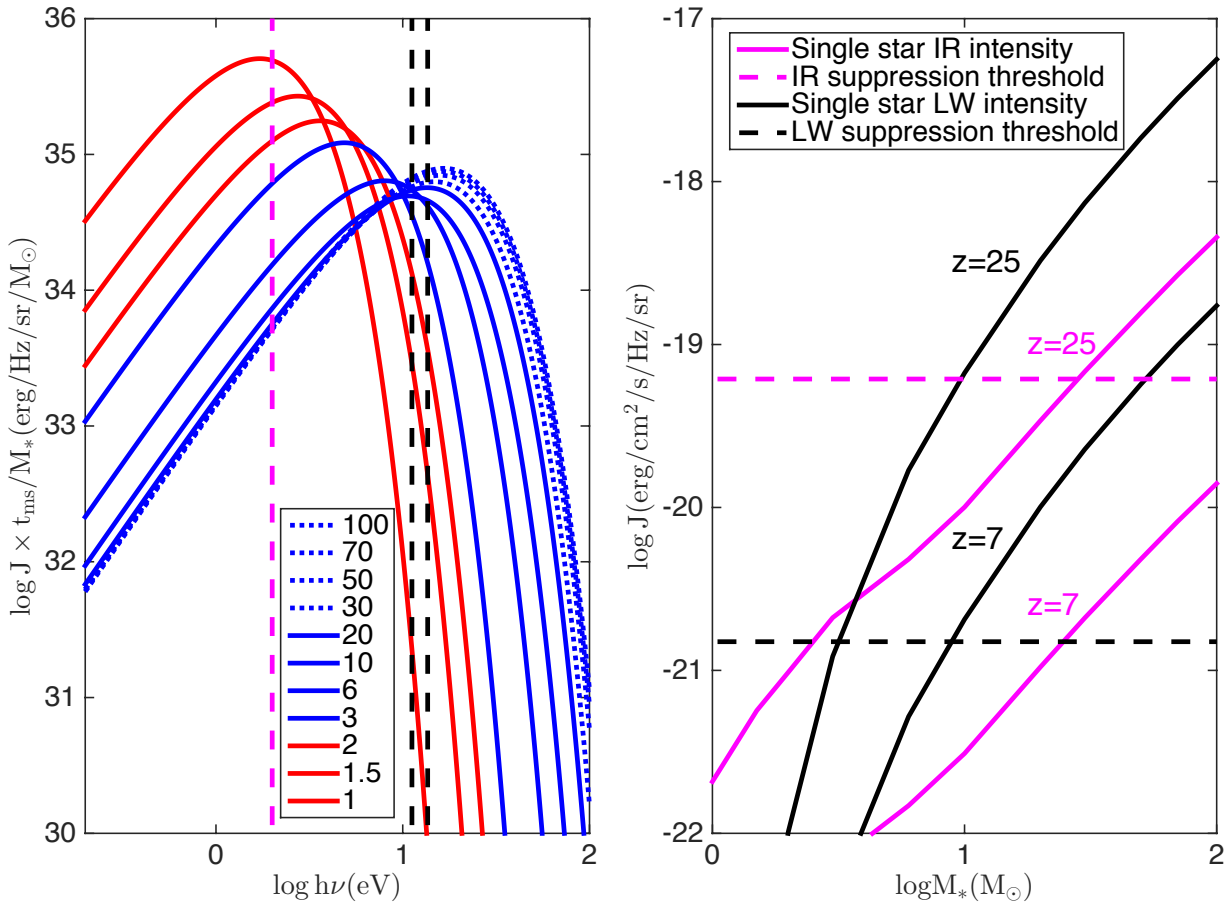

Fig. 1.— Left panel: shows the intrinsic black-body spectra of individual Pop-III stars per unit stellar mass, multiplied by the main sequence lifetime, for a set of stellar masses (in units of solar mass) indicated in the legend. Also shown as the vertical magenta dashed line is the photon energy of 2eV for the photo-detachment process. The LW band is indicated by the two black vertical dashed lines. Right panel: shows the radiation intensity at 2eV (magenta solid curves) and 11.2eV (black solid curves) for a single star of mass shown on the x-axis. The star is assumed to be located at the center and the intensity is measured at the core radius of the minihalo (see text for definition of core radius). Two cases are shown, one for a minihalo at $z = 25$ with virial temperature of 10^3 K (upper solid curves) and the other at $z = 7$ with virial temperature of 10^4 K (lower solid curves). For both IR and LW photons, no absorption is assumed for this illustration. The horizontal dashed lines with the same corresponding colors are the threshold intensity for complete suppression of $\mathrm{H_2}$ formation by the respective processes.

We consider the requirement of suppression of either $\mathrm{H_2}$ or $\mathrm{H^-}$ formation in the central core region of minihalos, which is likely most stringent compared to less dense gas at larger radii. Following Shapiro et al. (1999) we adopt the core radius and density to be $\mathrm{r_c} = \mathrm{r_v}/29.4$,

which is then

$$\mathrm{r_c} = 26.7\mathrm{h^{-1}pc}\left(\frac{\mathrm{T_v}}{1.98\times10^4\mathrm{K}}\right)^{\frac{1}{2}}\left(\frac{0.6}{\mu_\mathrm{P}}\right)^{\frac{1}{2}}\left(\frac{\Omega_\mathrm{m}}{\Omega_\mathrm{m}^\mathrm{z}}\frac{\Delta_\mathrm{c}}{18\pi^2}\right)^{-\frac{1}{2}}\left(\frac{1+\mathrm{z}}{10}\right)^{-\frac{1}{2}}. \quad (11)$$

and hydrogen number density in the core is $\mathrm{n_c} = 514\mathrm{n_v}$ ($\mathrm{n_v}$ is the gas number density at the virial radius):

$$\mathrm{n_c} = 4.5\mathrm{cm^{-3}}\left(\frac{1+\mathrm{z}}{10}\right)^3. \quad (12)$$

Since we use the numerical results from Wolcott-Green & Haiman (2012) on photo-detachment, it will be instructive to gain a physical understanding of its origin. The photodetachment cross section is

$$\sigma_- = 2.1\times10^{-16}\frac{(\epsilon-0.755)^{3/2}}{\epsilon^{3.11}}\mathrm{cm^2} \quad (13)$$

where ϵ is the photon energy in units of eV. The radiative association rate coefficient is $k_- = 1.3\times10^{-9}$cm^3 s^{-1}. Thus, with $\mathrm{J_{IR,crit}} = 6.1\times10^{-20}\mathrm{erg/s/cm^2/Hz/sr}$ at 2eV and minihalo core density of $\mathrm{n_c} = 31\mathrm{cm^{-3}}$ at $z = 18$ (see Equation 1) ($z = 18$ is used in Wolcott-Green & Haiman (2012)) and assuming that the spectrum shape of $\propto \nu^0$ in the range $0.755 - 13.6$eV, one finds that the ratio of photo-detachment rate to radiative association rate is 0.46; the ratio becomes 1.5 if one assumes the spectrum shape of $\propto \nu^{+1}$. Note that in the Raleigh-Jeans limit the spectral shape goes as $\propto \nu^{+2}$ (see Figure 1). We now see that when the photo-detachment rate and radiative association rate are approximately equal in the minihalo core, $\mathrm{H_2}$ formation is effectively completely suppressed, as one would have expected. This thus provides an order of magnitude understanding of the Wolcott-Green & Haiman (2012) results.

Given the expected little dust content in very metal poor gas in minihalos, the optical depth for IR photons at 2eV is negligible. As a numerical example, the core hydrogen column density would be $\mathrm{N_c} \equiv \mathrm{r_c n_c} = 1.5\times10^{20}\mathrm{cm^{-2}}$ for a minihalo of $\mathrm{T_v} = 10^4$ K at $z = 8$. Using the gas to dust column ratio (Draine 2003) with the assumption that dust content is linearly proportional to metallicity yields $A_V = 0.08(Z/\mathrm{Z_\odot})$ mag in this case. It is easy to see that we may safely neglect optical depth effect for IR photons in question. For LW photons, $\mathrm{H_2}$ self-shielding effect may be important. We include, conservatively, for maximum $\mathrm{H_2}$ self-shielding of LW radiation by placing all sources at the center of the minihalo with the self-shielding reduction of LW photons using the accurate fitting formula from Draine & Bertoldi (1996) for a halo at $z = 7$ with $T_v = 10^4$ K, corresponding Doppler parameter $b = 13\,\mathrm{km\,s^{-1}}$, $\mathrm{H_2}$ fraction of $\mathrm{f_{H_2}} = 10^{-3}$ and $\mathrm{H_2}$ column density equal to $\mathrm{f_{H_2} r_c n_c}$. This case is contrasted with the hypothetical case where self-shielding is neglected.

The left panel of Figure 2 shows the critical cumulative stellar mass required to completely suppress further star formation, as a function of the lower mass cutoff of the IMF $\mathrm{M_{low}}$, following a minihalo of $\mathrm{T_v} = 10^3$K at $z = 25$ through its becoming an atomic cooling halo at $z = 7$. In making this plot, we have adopted a Monte Carlo approach to randomly sample the IMF, assuming each starburst lasts about 4Myr, a time scale to approximate the effect of

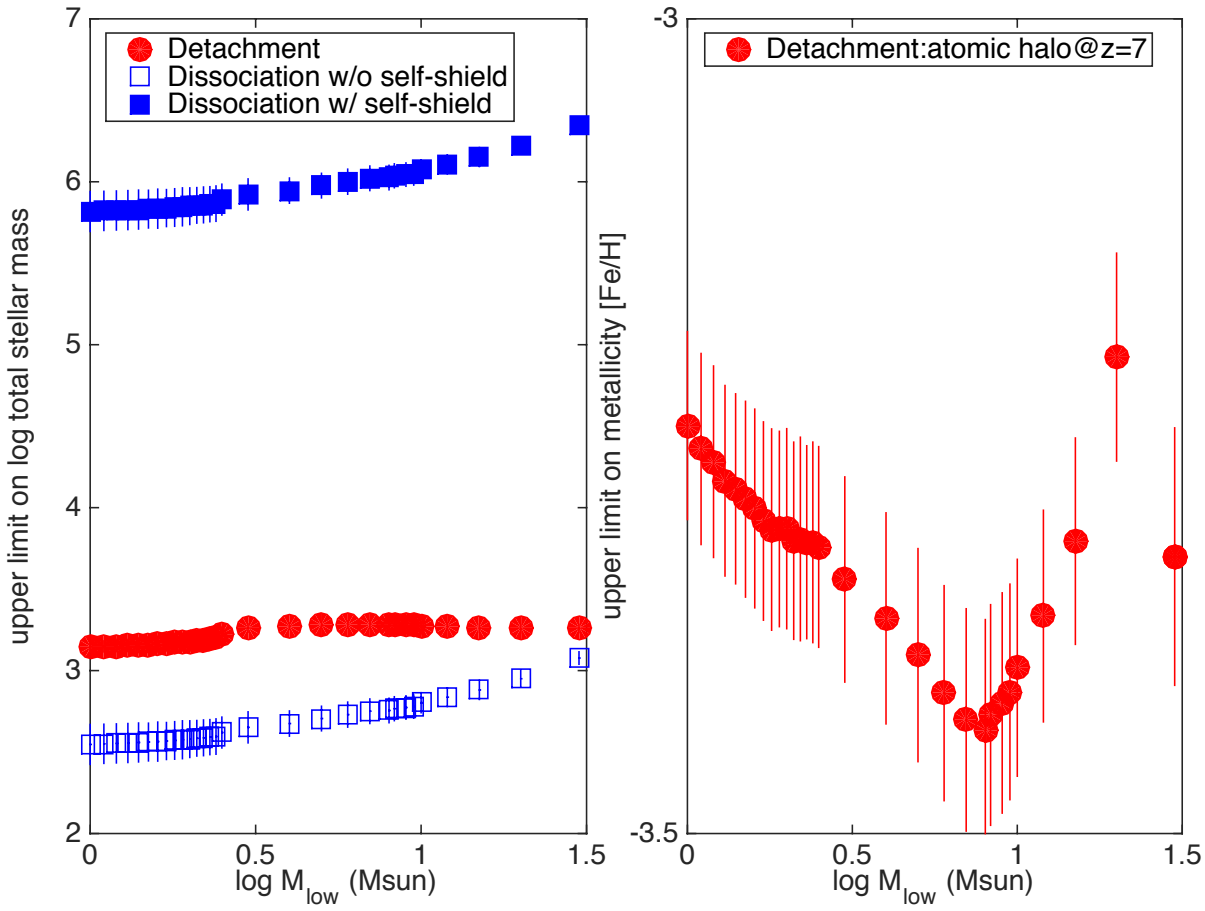

Fig. 2.— Left panel: shows the critical cumulative stellar mass for complete suppression of H_2 formation, as a function of the lower mass cutoff of the IMF M_{low}, via either the photo-dissociation process by LW photons with (blue open squares) and without H_2 self-shielding of LW photons (blue solid squares) or the photo-detachment process by infrared photons (red solid dots). In this example, we assume that a minihalo of virial temperature $T_v = 10^3$K is formed at $z = 25$ when star formation commences, and the critical stellar mass (i.e., upper limit on total stellar mass) is evaluated at $z = 7$ when the minihalo has grown to a virial temperature of $T_v = 10^4$K. Right panel: shows the upper bound on the mean gas metallicity, corresponding to the critical stellar mass shown in the left panel, evaluated at $z = 7$ when the minihalo has grown to a virial temperature of $T_v = 10^4$K. In both panels, the errorbars indicate the dispersions obtained by Monte Carlo realizations of different star formation histories, described in the text.

supernova blowout. While simulations have shown that the separation of episodic starbursts is about $20 - 100$Myr (e.g., Kimm & Cen 2014) for atomic cooling halos, we expect that the separations for minihalos would be larger, thanks to the more violent blowouts of gas by supernovae out of shallower potential wells and less efficient cooling in minihalos for gas return. To stay on the conservative side, we use temporal separations between star formation episodes of 20Myr. In general, a larger separation gives a lower total stellar mass, because the radiative

suppression effects are almost entirely dominated by stars formed within the ongoing starburst (not by stars from previous starbursts) and often the radiation from a single star is enough to provide the necessary suppression (see the right panel of Figure 1). On details regarding the Monte Carlo realizations, within each starburst, we randomly draw stars from the IMF with a lower mass cutoff of $\mathrm{M_{low}}$, until the radiation intensity in IR or UV, separately, at the core radius exceeds the required threshold. We keep track of stars formed in starbursts at higher redshift and take into account their radiative contributions given their main sequence lifetimes. Since we can not “draw" a fractional star, in cases where a single star would already exceed the required threshold, stellar mass is higher than if fractional stars can be drawn. Based on the Monte Carlo random sampling procedure to draw stellar distribution from the IMF, the obtained dispersion are shown as vertical bars on symbols in both panels of Figure 2.

It is evident that, taking into account $\mathrm{H_2}$ self-shielding of LW photons, for the entire range of $\mathrm{M_{low}}$ considered, the destructive effect due to photo-detachment is larger by two-three orders of magnitude than that due to photo-dissociation taking into account attenuation for LW photons. Thus, we will use the photo-detachment effect to place an upper bound on stellar mass that can form before further $\mathrm{H_2}$ formation hence star formation is completely suppressed. The amount of stars formed within minihalos is small, at $\sim 10^3\,\mathrm{M_\odot}$, prior to the minihalo becoming an atomic halo. This self-regulation of star formation in minihalos likely have a significant impact on the possible contribution of minihalos to reionization. A full characterization of this effect would need detailed simulations with this important process included. Wise et al. (2014) find stellar mass of $10^{3.5} - 10^{4.0}\,\mathrm{M_\odot}$ in minihalos of mass $10^{6.5} - 10^{7.5}\,\mathrm{M_\odot}$, which is approximately a factor of at least $3 - 10$ higher than allowed, even compared to the largest possible minihalos (before their becoming atomic cooling halos) considered here, as shown in the left panel of Figure 2. We note that the amount stars formed are a result of accumulation of the number of star formation episodes. We have "maximized" the stellar mass by using a conservative episodic interval and considering the maximum minihalos at a low redshift $z = 7$. Obviously, for smaller minihalos at higher redshift with longer “quiet" periods the amount of stellar mass formed will be smaller. This suggests that the contribution of stars formed in minihalos to reionization may be substantially reduced. We estimate that the contribution of minihalos to cosmological reionization photon budget is likely limited to a few percent.

Next, we consider the metal enrichment due to stars formed in minihalos. To compute that, we use the relation between the nickel (which decays to iron) mass produced by a supernova of mechanical explosion energy E:

$$\log \frac{\mathrm{M_{ni}}}{\mathrm{M_\odot}} = 1.49 \log \frac{\mathrm{E}}{10^{50}\,\mathrm{erg}} - 2.9 \tag{14}$$

(Pejcha & Prieto 2015) and the relation between explosion energy E and the main sequence stellar mass M:

$$\frac{\mathrm{E}}{10^{51}\,\mathrm{erg}} = (\frac{\mathrm{M}}{10.8\,\mathrm{M_\odot}})^2 \tag{15}$$

(Poznanski 2013). We assume all stars with main sequence mass above $8\,\mathrm{M}_\odot$ explode as supernavae, except the two intervals $17-23\,\mathrm{M}_\odot$ and $\geq 40\,\mathrm{M}_\odot$, which produce black holes based on the so-called compact parameter ξ as a physical variable (e.g., O'Connor & Ott 2011; Pejcha & Thompson 2015).

The right panel of Figure 2 shows the expected average metallicity when an atomic cooling halo is reached at $z=7$. corresponding to the critical stellar mass shown as solid red dots in the left panel of Figure 2. We see that, on average, the expected maximum metallicity due to stars formed in minihalos falls into the range of -3.3 ± 0.2 in solar units, for $\mathrm{M}_{\mathrm{low}}=1-30\,\mathrm{M}_\odot$. We use iron mass fraction of 1.77×10^{-3} as solar abundance (Asplund et al. 2009). We have conservatively assumed that enrichment process takes places in a closed-box fashion, with respect to metals produced. Furthermore, we have simplistically assumed that none of the metals produced is not incorporated back into subsequent stars. In reality, retainment of metals produced by stars in minihalos is probably far from complete, given their shallow potential wells, i.e., it is not a closed box. Furthermore, some of the earlier produced metals inevitably get reformed into stars. These conservative approaches used, along with our conservative adoption of 20Myr starburst separation, indicate that that the actual metallicity due to stars in minihalos may be significantly below the maximum allowed values indicated in the right panel of Figure 2. In other words, we expect that the metallicity floor put in by stars formed in previous minihalos, when an atomic cooling halo is formed, is likely significantly below -3.3 ± 0.2 in solar units.

There is one possible caveat in the arguments leading to the results. Despite the resultant low metallicity due to self-suppression of star formation by negative IR radiation feedback, the metallicity is not zero. Thus, it is prudent to check if the metallicity is sufficiently low to justify the neglect of low-temperature metal cooling. We find that, using $[\mathrm{Z/H}]=-3$ and molecular hydrogen fraction of $\mathrm{f_{H2}}=10^{-3}$, the ratio of the cooling rate of metal lines (primarily due to OI, CII, SiII aand FeII) to that of molecular hydrogen is found to be (4.1×10^{-2}, 1.6×10^{-3}, 2.6×10^{-4}) at temperature $\mathrm{T}=(10^3,10^{3.5},10^4)$ K (Maio et al. 2007), respectively. Empirically, experimental simulations have found that, in lieu of molecular hydrogen cooling, low-temperature metal cooling with a metallicity of $[\mathrm{Z/H}]\sim-1.5$ produces cooling effect comparable to that molecular hydrogen fraction with $\mathrm{f_{H2}}=10^{-3}$ (Kimm 2016, private communications), which is consistent with above estimates based on cooling rates. Thus, the low-temperature metal cooling is probably no more than $(\sim 2\%,\,0.1\%,\,0.01\%)$ of the molecular hydrogen cooling in the case of absent negative feedback examined here, if $[\mathrm{Z/H}]\leq-3.3$, in minihalos with virial temperatures $\mathrm{T_v}=(10^3,10^{3.5},10^4)$ K, respectively. Therefore, the low-temperature metal cooling is unlikely to be able to make up the "lost" H_2 cooling, due to negative feedback from local radiation, to alter the suppression of star formation.

3. Discussion and Conclusions

This study investigates the radiative feedback from resident stars in minihalos. We find that photo-detachment of H^- by infrared photons of energy $h\nu \geq 0.755$eV emitted by resident stars in minihalos is the most effective mechanism to suppress and hence self-regulate star formation within. The negative feedback effect due to Lyman-Werner photons would have been more effective, if the gas is transparent; however, H_2 self-shielding substantially reduces its effect to become subdominant to that of photo-detachment process.

We find that the amount of stars formed in minihalos is capped at about $10^3\,\mathrm{M}_\odot$, regardless of the lower mass cutoff of the initial mass function. As a result, it is shown that a stringent upper bound of metallicity of -3.3 ± 0.2 relative to the solar value due to stars formed in minihalos can be placed; the actual amount of stars and metallicity achieved by stars in minihalos may be significantly lower, because the various assumptions adopted, when needed, have been chosen to err, generously, on the conservative side to ensure that our results with respect to star formation in minihalos represent an upper bound.

The self-regulation of star formation in minihalos likely has a significant impact on the possible contribution of minihalos to reionization. In Kimm & Cen (2014, Figure 14) it is shown that, in the absence of significant contributions from minihalos with virial masses below $1.5 \times 10^8\,\mathrm{M}_\odot$, as an example, corresponding to minihalo threshold at $z = 9$ (see Equation 2), the reionization optical depth is expected to be no greater than 0.065. On the other hand, allowing for minihalos of masses as low as ($10^7\,\mathrm{M}_\odot$, $10^{6.5}\,\mathrm{M}_\odot$) to form stars unconstrained by this self-regulation physical process, the reionization optical depth would exceed $(0.075, 0.085)$, respectively, in general agreement with earlier results under similar assumptions with respect to dramatically increased contributions especially with very massive Pop III stars (e.g., Cen 2003a,b; Wyithe & Cen 2007). While these values are all consistent with the most recent Planck results (Planck Collaboration et al. 2015, $\tau_e = 0.066 \pm 0.016$) at $< 1.2\sigma$ level, upcoming results from Planck High-Frequency Instrument (HFI) data may provide a significant constraint on the star formation physics in minihalos.

The findings will also have profound ramifications on star formation and formation of supermassive black seeds in atomic cooling halos at high redshift, due to processes related to metal cooling, dust formation and fragmentation. As an example, low-temperature metal cooling may be suppressed (e.g., Bromm & Loeb 2003) to increase the probability of extending the formation of Pop III stars. Although simulations will be needed, this does suggest that, with a much lower mean metallicity, in conjunction with inhomogeneous metal enrichment processes, pockets of Pop III stars in atomic cooling halos may be more widespread than thought. The combination of a reduction of star formation in minihalo and a possible increase in stellar luminosity in atomic cooling halos (due to Pop III stars) will alter both the slope and cutoff of the luminosity function of galaxies at the faint end at the epoch of reionization (Kimm & Cen 2014; Trac et al. 2015). There may be two possible signatures in the luminosity function at the epoch of reionization. First, a possible steepening at the faint end right before a dramatic flat-

tening or downturn at the transition between the atomic cooling halo to minihalo mass may be expected; the steepening is due to the increased proportion of metal-free stars in lower mass atomic cooling halos. Second, due to generally increased variations in Pop III star fractions, in conjunction with stochastic starbursts, the shape of the luminosity function at the high end is likely to resemble powerlaws than exponential.

On a separate, but potentially related subject, we note that metallicities of stars in both types of globular clusters, in the bimodal metallicity distribution (e.g., Forbes et al. 1997; Harris et al. 2006), are significantly higher than -3. This indicates that, in scenarios where globular clusters are formed in dwarf, atomic cooling galaxies (Kimm et al. 2016), most of the metals ought to originate from previous generation of stars formed in either other and/or progenitor atomic cooling halos prior to forming globular clusters at the centers of these dwarf galaxies. Given the much reduced star formation hence metallicity in minihalos, it would seem conceivable that Pop III stars formed in atomic cooling halos may make a significant contribution to the pre-enrichment (of, say, Fe) of the gas forming the first-generation stars in globular clusters.

I thank Zoltan Haiman, Kohei Inayoshi, Taysum Kimm, John Wise and Jemma Wolcott-Green for useful discussion and communications, Paola Marigo for stellar track data, Alexander Heger, Berhnard Mueller and Ondrej Pejcha for educational discussion on supernova related issues, and Umberto Maio for sharing low temperature cooling data files. This work is supported in part by grants NNX12AF91G and AST15-15389.

REFERENCES

Abel T., Bryan G. L., Norman M. L., 2002, Science, 295, 93

Asplund M., Grevesse N., Sauval A. J., Scott P., 2009, ARA&A, 47, 481

Bromm V., Loeb A., 2003, ApJ, 596, 34

Bromm V., Coppi P. S., Larson R. B., 2002, ApJ, 564, 23

Cen R., 2003a, ApJ, 591, 12

Cen R., 2003b, ApJ, 591, L5

Chuzhoy L., Kuhlen M., Shapiro P. R., 2007, ApJ, 665, L85

Draine B. T., 2003, ARA&A, 41, 241

Draine B. T., Bertoldi F., 1996, ApJ, 468, 269

Forbes D. A., Brodie J. P., Grillmair C. J., 1997, AJ, 113, 1652

Harris W. E., Whitmore B. C., Karakla D., Okoń W., Baum W. A., Hanes D. A., Kavelaars J. J., 2006, ApJ, 636, 90

Hirano S., Hosokawa T., Yoshida N., Umeda H., Omukai K., Chiaki G., Yorke H. W., 2014, ApJ, 781, 60

Hirano S., Hosokawa T., Yoshida N., Omukai K., Yorke H. W., 2015, MNRAS, 448, 568

Kimm T., Cen R., 2014, ApJ, 788, 121

Kimm T., Cen R., Rosdahl J., Yi S., 2016, preprint, (arXiv:1510.05671, in press of MNRAS)

Machacek M. E., Bryan G. L., Abel T., 2001, ApJ, 548, 509

Maio U., Dolag K., Ciardi B., Tornatore L., 2007, MNRAS, 379, 963

Marigo P., Girardi L., Chiosi C., Wood P. R., 2001, A&A, 371, 152

Nakamura F., Umemura M., 2002, ApJ, 569, 549

O'Connor E., Ott C. D., 2011, ApJ, 730, 70

O'Shea B. W., Norman M. L., 2008, ApJ, 673, 14

Pejcha O., Prieto J. L., 2015, preprint, (arXiv:1501.06573)

Pejcha O., Thompson T. A., 2015, ApJ, 801, 90

Planck Collaboration et al., 2015, preprint, (arXiv:1502.01589)

Poznanski D., 2013, MNRAS, 436, 3224

Shapiro P. R., Iliev I. T., Raga A. C., 1999, MNRAS, 307, 203

Trac H., Cen R., Mansfield P., 2015, ApJ, 813, 54

Wise J. H., Abel T., 2007, ApJ, 671, 1559

Wise J. H., Demchenko V. G., Halicek M. T., Norman M. L., Turk M. J., Abel T., Smith B. D., 2014, MNRAS, 442, 2560

Wolcott-Green J., Haiman Z., 2012, MNRAS, 425, L51

Wyithe J. S. B., Cen R., 2007, ApJ, 659, 890

This preprint was prepared with the AAS LaTeX macros v5.2.